Metrol. Meas. Syst., Vol. 27 (2020) No. 2, pp. 289–300
DOI: 10.24425/mms.2020.132775

PAN POLSKA AKADEMIA NAUK

METROLOGY AND MEASUREMENT SYSTEMS

Index 330930, ISSN 0860-8229
www.metrology.wat.edu.pl

M&MS

DESIGN AND NUMERICAL ANALYSIS OF A HIGHLY SENSITIVE ULTRASONIC ACOUSTIC SENSOR BASED ON π-PHASE-SHIFTED FIBER BRAGG GRATING AND FIBER MACH–ZEHNDER INTERFEROMETER INTERROGATION

Krishna Mohan Dwivedi[1)], Gaurav Trivedi[1)], Sunil K. Khijwania[2)], Tomasz Osuch[3,4)]

1) *Indian Institute of Technology Guwahati, Department of Electronics and Electrical Engineering, Guwahati, India* (*krishna.dwivedi@iitg.ac.in*, *trivedi@iitg.ac.in*)
2) *Indian Institute of Technology Guwahati, Department of Physics, Guwahati, India* (*skhijwania@iitg.ac.in*)
3) *Warsaw University of Technology, Faculty of Electronics and Information Technology, Institute of Electronic Systems, Nowowiejska 15/19, 00-665 Warsaw, Poland* (✉ *t.osuch@elka.pw.edu.pl*, +48 22 234 7741)
4) *National Institute of Telecommunications, Szachowa 1, 04-894 Warsaw, Poland*

Abstract

A π-phase-shifted fiber Bragg grating (π-FBG) shows high sensitivity to the ultrasonic (US) wave as compared to the conventional FBG due to the strong slow-light phenomenon at the resonance peak. However, its sensitivity is limited by the interrogation schemes. A combination of π-FBG and unbalanced fiber Mach–Zehnder interferometer (F-MZI) are theoretically analyzed and optimized for the highly sensitive acoustic sensor. The coupled-mode theory (CMT) and transfer matrix method (TMM) are used to establish the numerical modelling of π-FBG. For the optimized grating parameters of π-FBG, the proposed sensing system shows the high strain sensitivity of 1.2×10^8 /ε, the highest dynamic strain resolution of 4.1fε/$\sqrt{\text{Hz}}$, and the highest wavelength shift resolution of 4.9×10^{-9} pm. Further, the proposed sensing system strongly supports both time and wavelength division multiplexing techniques. Therefore, the proposed sensing system shows extreme importance in single as well as quasi-distributed US acoustic wave sensing networks.

Keywords: π-FBG, unbalanced F-MZI, strain sensitivity, ultrasonic acoustic sensor.

1. Introduction

Over the last few years, fiber-optic ultrasonic sensors have attracted massive attention in various real field applications including – but not limited to – *structural health monitoring* (SHM) of civil infrastructures and aerospace structures, medical diagnostics, *etc*., due to their numerous advantages over lead-zirconate-titanate ultrasonic sensors such as capability of multiplexing, immunity to electromagnetic and radio frequency interference, ability to work in harsh environments, remote sensing, *etc*. [1, 2]. Among the various fiber-optic ultrasonic sensors reported in the literature, *fiber Bragg grating* (FBG) based are the ones most frequently used for SHM and non-destructive testing [1, 2]. It is because FBG exhibits inherent properties of wavelength encoding

nature, which provides excellent multiplexing techniques, being small in size and easily embedded into the structural material without degradation of material integrity for real-time sensing [3–11]. The working principle of most FBG acoustic sensors is based on wavelength modulation in which the dynamic ultrasonic strain wave shifts the Bragg wavelength. The theoretical and experimental studies show that FBG is hardly sensitive to the *ultrasonic* (US) wave whose wavelength is smaller than the grating length [12, 13]. The typical ratio between the grating length and the ultrasonic wavelength obtained is 1/7 for the high sensitivity acoustic sensor [14]. Therefore, for the high frequencies of acoustic ultrasonic wave detection, a short length FBG is needed. However, the short length gratings suffer from low detection sensitivity due to their reduced peak reflectivity and very moderate reflectivity slope. Recently, Liang et al. have proposed the novel side-lobe modulation for high frequencies of ultrasonic waves [15]. However, the proposed sensor shows a weak optical signal and offers low sensitivity. A sensor having high sensitivity along with a broad bandwidth inspection would be of extreme importance for ultrasonic detection.

A *π-phase-shifted* FBG (π-FBG) is a special kind of FBG whose reflected spectra have a strong transmission resonance at the Bragg wavelength due to a π-phase shift in the center of refractive index change. It shows better sensitivity and is capable of detecting the megahertz frequency range of ultrasonic signals [16, 17]. Due to strong resonance, a slow-light phenomenon is observed in π-FBG at Bragg wavelength which increases the optical path length and, thus, enhanced sensitivity is achieved [18, 19]. Further, light is confined in the phase-shifted area, which reduces the effective length of the grating and enables the π-FBG to detect megahertz frequencies. Therefore, in recent years, several ultrasonic sensors based on π-FBG have been proposed for the real-time SHM measurements [20–23]. Various approaches have been proposed for interrogating the Bragg wavelength shift of a π-FBG caused by ultrasonic waves. The transmitted/reflected light of the π-FBG is detected with a single photodetector [17]. However, the sensitivity of the system is limited by the laser source's (intensity and frequency) noise level. To minimize the laser intensity noise, the Pound–Drever–Hall technique can be used [20]. Still, this technique has significant disadvantages *i.e.* it is expensive, bulky, and very complicated in practical realization. Moreover, such a sensing system shows very weak multiplexing techniques. Hence, a balanced photodetector technique was proposed to eliminate the laser intensity noise [21]. The proposed sensing system is straightforward, low cost and offers multiplexing techniques. Yet, its sensitivity is limited by the laser frequency noise and photodetector noise. Hu et al. presented an imbalanced fiber-optic Michelson interferometer as a reference channel to reduce the laser intensity noise as well as laser frequency noise of a π-FBG based acoustic emission sensor system [22]. The proposed sensing system offers multiplexing techniques but the sensitivity is restricted by the photo-detectors' noise. An ultrasonic sensor based on two cascaded π-FBGs that provide multiplexing capabilities is demonstrated in [23]. This sensing scheme is based on the *broadband light source* (BLS); therefore, the cost of the system is relatively low as compared to the laser-based sensing approach. However, it suffers from low sensitivity due to the high-intensity noise of the BLS.

Interrogation with an unbalanced *fiber Mach–Zehnder interferometer* (F-MZI) is known for high resolution, high sensitivity as well as broad bandwidth detecting scheme for the Bragg wavelength shifts caused by the dynamic wave [24–27]. Moreover, it allows both the time division as well as wavelength division multiplexing techniques [24, 25, 27]. An F-MZI converts the shift in the Bragg wavelength, $\Delta\lambda_B$, of FBG into the intensity change. The change in intensity is proportional to $\Delta\lambda_B$, and path-length mismatch d of the F-MZI. Therefore, the sensitivity of the F-MZI can be increased by increasing the d. However, the maximum path-length mismatch cannot exceed the coherent length of the signal in the fiber. The coherent length is inversely proportional to the bandwidth of the reflected signal from the FBG, which is ultimately dependent on the index change. An F-MZI shows limited sensitivity with the conventional FBGs due to their broader

Metrol. Meas. Syst., Vol. 27 (2020), No. 2, pp. 289–300
DOI: 10.24425/mms.2020.132775

bandwidth (> 80 pm). In this paper, we theoretically analyze and optimize an ultrasonic acoustic sensor based on the π-FBG and F-MZI interrogation scheme for single and quasi-distributed sensing networks. To do so, first, we optimize the π-FBG for grating parameters, *i.e.* grating length (L) and index change (Δn). In most of the practical applications, the grating length of 5 mm is used [15, 16, 21, 23]. To optimize the index change of the π-FBG sensor, the *optical path difference* (OPD) of the F-MZI, which is a product of the refractive index of fiber and path-length mismatch, should be considered. The OPD is also inversely proportional to the spectral bandwidth of the signal fed into the F-MZI. The maximum OPD of 96 m is reported in [25] for the fiber laser sensor, to the best of authors' knowledge. The optimum index change is taken as 1.2×10^{-3}. For the optimum grating parameters (L = 5 mm and $\Delta n = 1.2 \times 10^{-3}$), the π-FBG is characterized by the peak transmissivity of 0.985 and *full width at half maximum* (FWHM) of 0.012 pm. The OPD of the F-MZI is calculated at 76.01 m for the given FWHM. A high strain sensitivity of $1.2 \times 10^{8}/\varepsilon$ and a high strain resolution of 4.1 f$\varepsilon/\sqrt{\text{Hz}}$ are achieved from the proposed sensing system. The achieved strain resolution of the proposed sensing system is much better than 7.3 f$\varepsilon/\sqrt{\text{Hz}}$ of [25] and provides a wavelength shift resolution of 4.9×10^{-9} pm. A wavelength shift resolution of 3.7×10^{-3} pm is reported in [22] for an acoustic-emission sensor based on the π-FBG and a Michelson interferometer. Our sensing scheme shows a much better wavelength resolution than reported in [22]. Furthermore, the intensity noise of BLS in the proposed sensing system can be easily eliminated by using a dual-channel F-MZI configuration [28].

2. Theoretical Modelling

2.1. Acoustic-Ultrasonic Wave Modelling

Acoustic emission is a transient ultrasonic wave with typical frequency varying from 100 kHz to 1 MHz and generated by damage-related structural changes, such as surface degradation, defect initiation, crack growth, *etc*. [1]. A longitudinal US acoustic wave can be considered as a sinusoidal strain wave which can be given as [12]

$$\varepsilon(t) = \varepsilon_m \cos\left(\frac{2\pi}{\lambda_S} z - \omega_S t\right), \tag{1}$$

where ε_m is the US acoustic strain field amplitude normalized to the US acoustic wavenumber $2\pi/\lambda_S$, λ_S, and ω_S are wavelength and angular frequency of US acoustic wave, respectively, z is the direction of US wave, and t is instant time.

An FBG is a permanent periodic induced refractive index change along the finite length of the fiber. The variation of the effective refractive index of fiber along the grating length L is given as

$$n_{eff}(z) = n_{eff} + \overline{\delta n}\left(1 + \nu \cos\left[\frac{2\pi}{\Lambda} z + \phi(z)\right]\right), \quad 0 \le z \le L, \tag{2}$$

where n_{eff} is the effective refractive index of fiber in the absence of grating; $\overline{\delta n}$ denotes the averaged index change for a single grating period; ν stands for fringe visibility of index change; Λ is period of grating and $\phi(z)$ is grating chirp. Due to this periodic perturbation, a portion of input light is reflected by the FBG and the remaining light is passed through it. The reflected/transmitted light has a central wavelength known as the Bragg wavelength which is a multiplication of effective refractive index and grating period and can be given as

$$\lambda_B = 2 n_{eff} \Lambda. \tag{3}$$

FBGs are inherently sensitive to strain and temperature. FBG measures all other possible physical parameters which can be mapped into strain or temperature domains. The shift in the Bragg wavelength of the FBG due to the change in strain and temperature is given as [30]

$$d\lambda = (K_\varepsilon \Delta\varepsilon + K_T \Delta T)\, \lambda_B\,, \tag{4}$$

where $K_\varepsilon \approx 0.78 \times 10^{-6}\varepsilon^{-1}$, and $K_T \approx 8.6 \times 10^{-6}\,^{\circ}\mathrm{C}^{-1}$ are strain and thermal sensitivity coefficients, respectively. Terms $\Delta\varepsilon$ and ΔT denote changes in strain and in temperature, respectively.

When longitudinal US acoustic wave, as described in (1), propagates through the FBG, it changes the effective refractive index and the period of grating. The period of grating is changed due to the geometric effect. The change in the z-axis is translated to the z'-axis according to the following formula [12]:

$$z' = f(z,t) = z + \varepsilon_m \frac{\lambda_s}{2\pi}\left[\sin\left(\frac{2\pi}{\lambda_s}z - \omega_s t\right) + \sin(\omega_s t)\right]. \tag{5}$$

The change in the refractive index is due to the elasto-optic effect and can be expressed as [12]:

$$\Delta n'(z',t) = -\left(\frac{n_{eff}^3}{2}\right)\cdot\left[P_{11} - \mu\left(P_{11}+P_{12}\right)\right]\cdot\varepsilon_m \cos\left(\frac{2\pi}{\lambda_s}z' - \omega_s t\right), \tag{6}$$

where P_{11} and P_{12} are stress-optics coefficients, and μ is the Poisson's ratio. From (2), (5), and (6), the new effective refractive index under US wave is given as

$$\begin{aligned} n'_{eff}(z',t) = {} & n_{eff} + \overline{\delta n}\left(1 + \nu\cos\left[\frac{2\pi}{\Lambda}f^{-1}(z',t)\right]\right) \\ & -\left(\frac{n_{eff}^3}{2}\right)\cdot\left[P_{11} - \mu(P_{11}+P_{12})\right]\cdot\varepsilon_m\cos\left(\frac{2\pi}{\lambda_s}z' - \omega_s t\right). \end{aligned} \tag{7}$$

2.2. Analysis of π-FBG under US wave using the Transfer Matrix Method

In this paper, the *transfer matrix method* (TMM) [29] is used to simulate the π-FBG for US wave. In this approach, grating length L is divided into N uniform sections of length δl ($\delta l \gg \Lambda$), and constant values of κ and σ are assigned to each uniform section. The transfer matrix of i-th section is described as

$$T_i = \begin{bmatrix} T_{11i} & T_{12i} \\ T_{21i} & T_{22i} \end{bmatrix} = \begin{bmatrix} \cosh(\Omega_i \delta l_i) - i\dfrac{\overline{\sigma}}{\Omega_i}\sinh(\Omega_i\delta l_i) & -i\dfrac{\kappa_i}{\Omega_i}\sinh(\Omega_i\delta l_i) \\ i\dfrac{\kappa_i}{\Omega_i}\sinh(\Omega_i\delta l_i) & \cosh(\Omega_i\delta l_i) + i\dfrac{\overline{\sigma}}{\Omega_i}\sinh(\Omega_i\delta l_i) \end{bmatrix}, \tag{8}$$

where $\Omega_i = \sqrt{\kappa_i^2 - \overline{\sigma}_i^2}$, and $\overline{\sigma}$ is general DC self-coupling coefficient is defined as

$$2\pi n_{eff}\left(\frac{1}{\lambda} - \frac{1}{\lambda_B}\right) + \frac{2\pi}{\lambda}\overline{\delta n}.$$

Metrol. Meas. Syst., Vol. 27 (2020), No. 2, pp. 289–300
DOI: 10.24425/mms.2020.132775

The overall response of π-FBG is given as

$$\begin{bmatrix} R_{fN} \\ R_{bN} \end{bmatrix} = [T_N][T_{N-1}]\cdots\left[T_{ps}\right]\cdots[T_2][T_1]\begin{bmatrix} R_{f0} \\ R_{b0} \end{bmatrix} = \left(\prod_{i=1}^{N} T_i\right)\begin{bmatrix} R_{f0} \\ R_{b0} \end{bmatrix} \tag{9}$$

where R_{f0} and R_{b0} are the input forward, and backward field amplitudes, respectively, and R_{fN} and R_{bN} correspond to output field amplitudes. T_{ps} is the phase-shift matrix and can be given as [29]

$$T_{ps} = \begin{bmatrix} e^{-i\phi/2} & 0 \\ 0 & e^{i\phi/2} \end{bmatrix}, \tag{10}$$

where ϕ is the shift in the phase of grating and defined as $\phi/2 = 2\pi n_{eff}\Delta z/\lambda$, Δz stands for the separation between two grating sections. Applying the appropriate boundary conditions ($R_{f0} = 1$ and $R_{bN} = 0$) in (9), the reflection and transmission coefficients of the grating are calculated as

$$\rho = \frac{T_{21}}{T_{11}}, \tag{11}$$

$$t = \frac{1}{T_{11}}. \tag{12}$$

2.3. System Modelling

The proposed sensing system is shown in Fig. 1. The transmitted spectrum of π-FBG is very complicated and contains many peaks, as shown in Fig. 1, and as such cannot be directly interrogated by the F-MZI. Therefore, an optimized *apodized* FBG (AFBG) is used to filter out the narrow peaks of π-FBG spectra at the Bragg wavelength under the US acoustic wave. A chirped FBG can be also used for this purpose because it also has a top-hat reflection spectrum. However, the (relatively small) chirp rate and an appropriate grating length should be chosen to ensure a high reflection coefficient and desired spectral width. The filtered peak holds the entire

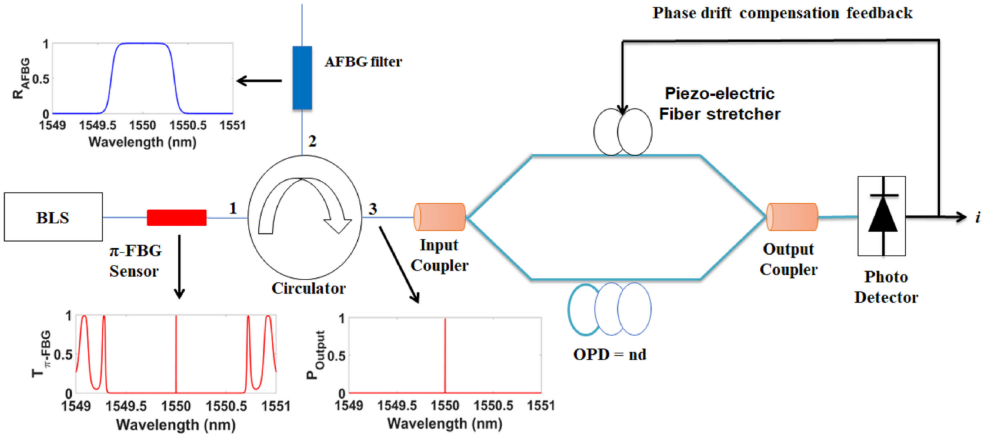

Fig. 1. Schematic of π-FBG ultrasonic acoustic sensor using interferometric interrogation technique.

characteristics of π-FBG and acts as source input to the interferometer. A circulator is used to direct the light from port 1 to port 2 and from port 2 to port 3 in clockwise direction.

The output filter power at port 3 of the circulator is given as

$$P_{filter\text{-}out} = \int P_0(\lambda) T_{\pi\text{-}sensor}(\lambda) R_{\mathrm{AFBG}}(\lambda) \mathrm{d}\lambda, \tag{13}$$

where P_0 is the *broadband light source* (BLS) output optical power, $T_{\pi\text{-}sensor}$ denotes the transmissivity of the π-FBG sensor and R_{AFBG} is the reflectivity of AFBG filter. The F-MZI output power is the coherent sum of fields traveling in both lower and upper arms. For the ideal 50% coupling at both F-MZI couplers, the output power is given as

$$P = P_{filter\text{-}out} \left(1 + 0.5 \cos\left(\psi(\lambda) + \phi\right)\right), \tag{14}$$

where $\psi(\lambda) = 2\pi nd/\lambda$ is the phase difference due to the path-length imbalance of the F-MZI, d is the path-length mismatch between the fiber arms, n is the effective index of the fiber core, and ϕ is a bias phase offset of the F-MZI. The F-MZI sensitivity is maximum for the phase bias of $\pi/2$. For the US strain perturbation, the term detected at the output of the sensor is the second term of the (14). Thus, (14) becomes

$$P = 0.5 P_{filter\text{-}out}\, \psi(\lambda). \tag{15}$$

The US strain wave modulates the Bragg wavelength of π-FBG; therefore, the phase of the F-MZI is also changed. The change in the phase is given as

$$\Delta\psi(\lambda) = \frac{2\pi nd}{\lambda^2} \Delta\lambda_B, \tag{16}$$

where $\Delta\lambda_B$ is the change in the Bragg wavelength due to US acoustic waves. The product nd, in the above equation, is known as the *optical path difference* (OPD). For the maximum sensitivity, the optimum OPD satisfies the condition OPD $\times\, \delta$k = 2.355 [24], where δk presents the spectral bandwidth of optical signal (express in wavenumber/unit) fed to the F-MZI.

The strain sensitivity, S_ε, of the system is given as

$$S_\varepsilon = \frac{1}{P_{filter\text{-}out}} \frac{\mathrm{d}P}{\mathrm{d}\varepsilon} = \frac{1}{P_{filter\text{-}out}} \frac{\mathrm{d}P}{\mathrm{d}\psi} \frac{\mathrm{d}\psi}{\mathrm{d}\lambda} \frac{\mathrm{d}\lambda}{\mathrm{d}\varepsilon} = \frac{\pi nd}{\lambda^2} \Delta\lambda_B\,. \tag{17}$$

3. Numerical results and discussion

In this section, we first optimize the π-FBG for the optimum OPD of the F-MZI. We also assume that the grating is lossless. The lossy grating has a low transmissivity peak and wide FWHM at the Bragg wavelength [18, 19]. The wider FWHM, the lower the OPD value, and thus the sensitivity of the sensing system is reduced as stated in (17). The typical length of grating is taken as 5 mm. Figure 2 shows the change in the resonance peak transmissivity of π-FBG with index change. For better detection or signal to noise ratio, the resonance peak transmissivity must be as high as possible [22]. As the index change increases, the transmissivity decreases. It is due to the increase in the diffraction efficiency of the grating. Therefore, a light start reflected out at the initial length of the grating as the index change increased. The full width at half maximum of the transmission resonance peak decreases linearly on the logarithmic scale with the index change increasing, as shown in Fig. 3. The importance of bandwidth of resonance peak

Metrol. Meas. Syst., Vol. 27 (2020), No. 2, pp. 289–300
DOI: 10.24425/mms.2020.132775

is that it determines the OPD of the F-MZI. As discussed in the previous section, the OPD is inversely proportional to the spectral bandwidth of the signal. The OPD is linearly increased on the logarithmic scale as the index change is increased as shown in Fig. 4. In the literature, an F-MZI having maximum OPD of 96 m was used to interrogate the fiber laser-based sensor [25], to the best of authors' knowledge. Considering the maximum limit of this OPD, we choose the index change of 1.2×10^{-3}. For the optimum grating parameters, the π-FBG is characterized by the peak transmissivity of 0.985 and FWHM of 0.012 pm. The OPD of the F-MZI is calculated as 76.01 m for the given FWHM.

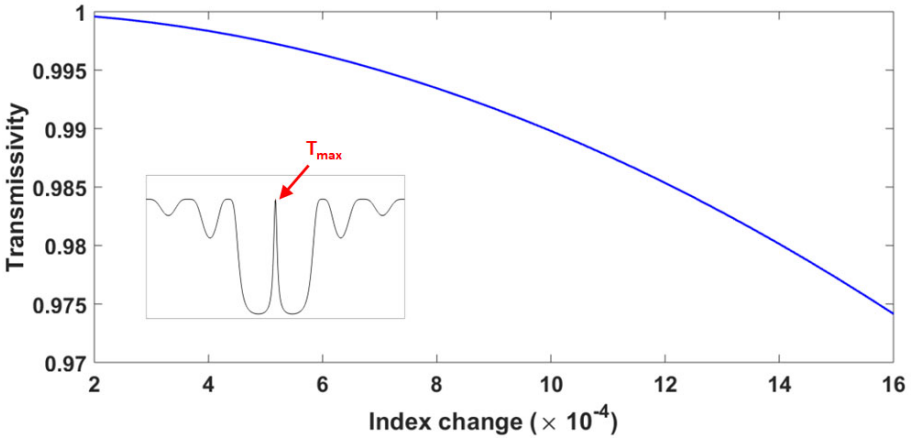

Fig. 2. Transmissivity vs. index change for fixed $L = 5$ mm (inset figure shows the peak transmissivity of π-FBG at Bragg wavelength).

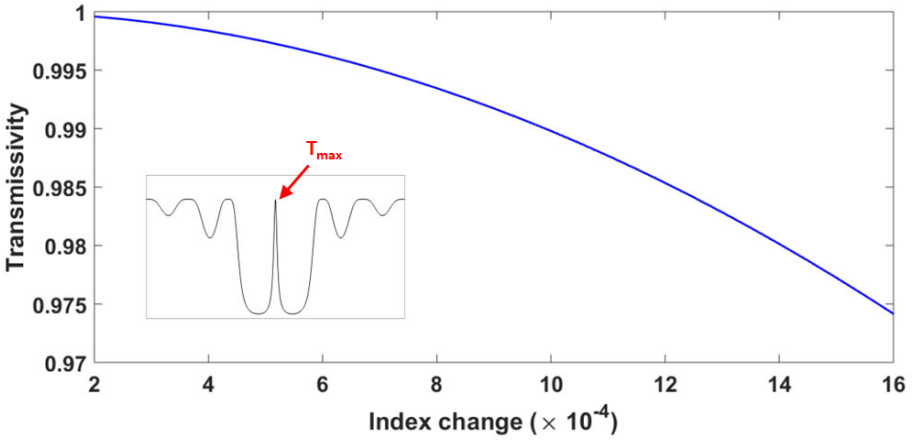

Fig. 3. FWHM of resonance peak of π-FBG vs. index change for fixed $L = 5$ mm (inset figure shows the FWHM of π-FBG at Bragg wavelength).

As stated in (17), the strain sensitivity of the F-MZI is proportional to the Bragg wavelength shift of π-FBG. The shift in the Bragg wavelength not only depends upon US strain amplitude, but it is also highly dependent on the US acoustic wavelength, λ_S [12]. Figure 5 shows the

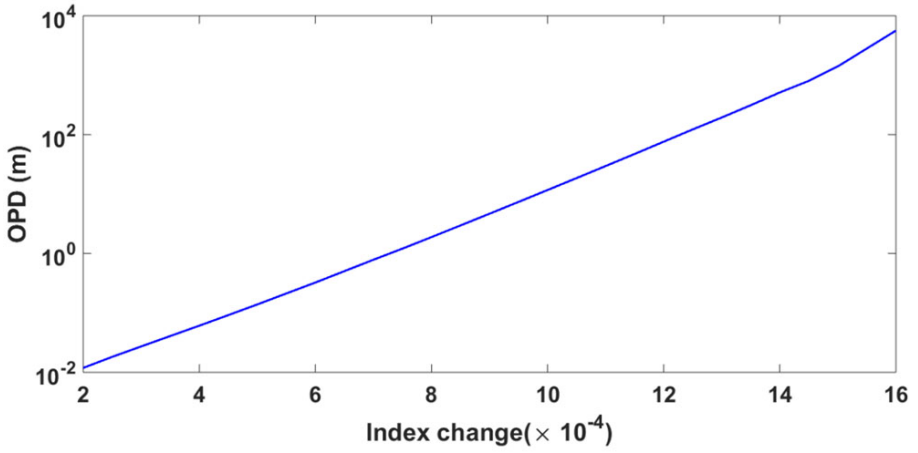

Fig. 4. OPD of the F-MZI vs. index change.

temporal wavelength shift sensitivity S_λ, (*i.e.*, instant time, t, is varying from 0 to US period $2\pi/\lambda_S$), which is defined as the ratio of magnitude of change in Bragg wavelength under US acoustic wave to the Bragg wavelength shift under the static strain and can be expressed as $S_\lambda\,(\lambda_S/L,\,\varepsilon_m) = \Delta\lambda_{\mathrm{US}}\,(\lambda_S/L,\,\varepsilon_m)\,/(\lambda_{B0}\varepsilon_m)$, of the optimized π-FBG as a function of λ_S/L for the strain amplitude of 100 με. The optimized π-FBG achieves a constant sensitivity for the ratio $\lambda_S/L > 2$, which is five times lower than the result achieved by Minardo *et al.* [12] and 3.5 times lower than in [14].

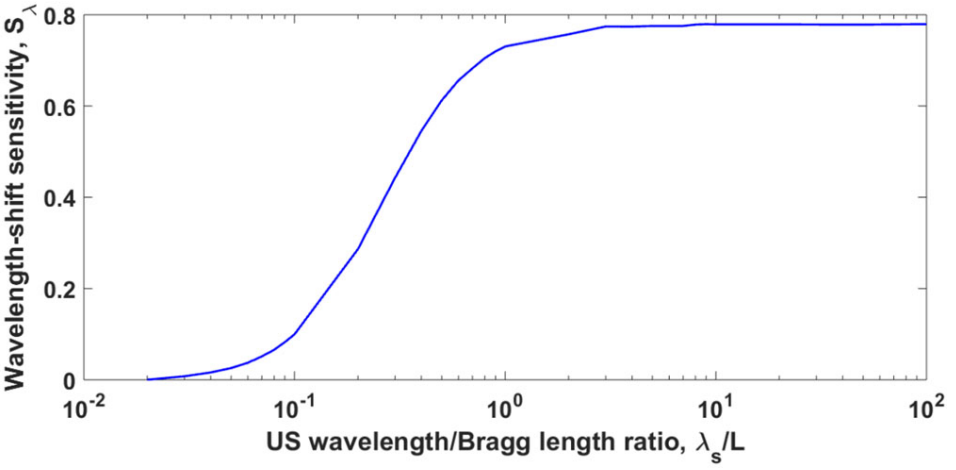

Fig. 5. Bragg wavelength shift sensitivity of π-FBG, S_λ vs. the US wavelength for the strain amplitude of 100 με.

The strain sensitivity of the F-MZI for the optimized OPD of 76.1 m is shown in Fig. 6. The maximum strain sensitivity of $1.2\times10^8/\varepsilon$ is obtained for the ratio $\lambda_S/L > 2$. The maximum phase sensitivity ($\Delta\psi/\Delta\varepsilon$) which corresponds to the maximum strain sensitivity is calculated at 240 rad/με. Currently, the F-MZI can detect a high-resolution dynamic phase shift of 1 μrad/$\sqrt{\text{Hz}}$

Metrol. Meas. Syst., Vol. 27 (2020), No. 2, pp. 289–300
DOI: 10.24425/mms.2020.132775

[24], which gives a high dynamic strain resolution of 4.1 fε/√Hz for the given phase shift sensitivity. The strain resolution of the proposed sensing system is nearly half as compared to the strain resolution of 7.3fε/√Hz of the fiber laser sensor reported in [25]. Further, for the achieved strain resolution of 4.1 fε, a wavelength shift resolution of 4.92×10^{-9} pm is easily obtained. A wavelength shift resolution of 3.7×10^{-3} pm is given in [22] for the acoustic-emission sensor based on the π-FBG and a Michelson interferometer. The proposed sensor shows a much better wavelength resolution than that presented in [22].

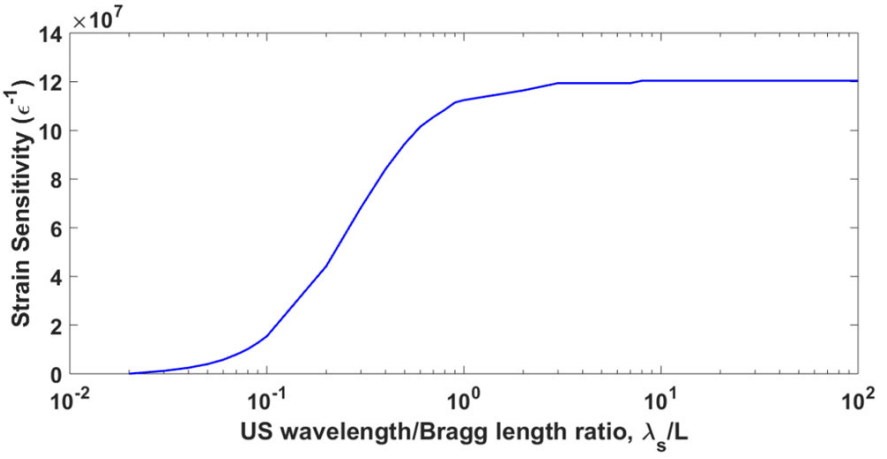

Fig. 6. Strain sensitivity of π-FBG, S_ε vs. the US wavelength for the strain amplitude of 100 με.

Figure 7 shows the shift in Bragg wavelength and wavelength-shift sensitivity of optimized π-FBG for the US acoustic strain amplitudes. The ratio of the US wavelength to the grating length (λ_S/L) is taken as 3. A linear shift in the Bragg wavelength having a slope of 1.2 pm/με and constant wavelength-shift sensitivity of 0.774 are achieved. The result shows that for the ratio $\lambda_S/L > 2$, the proposed π-FBG experiences uniform distribution of strain along

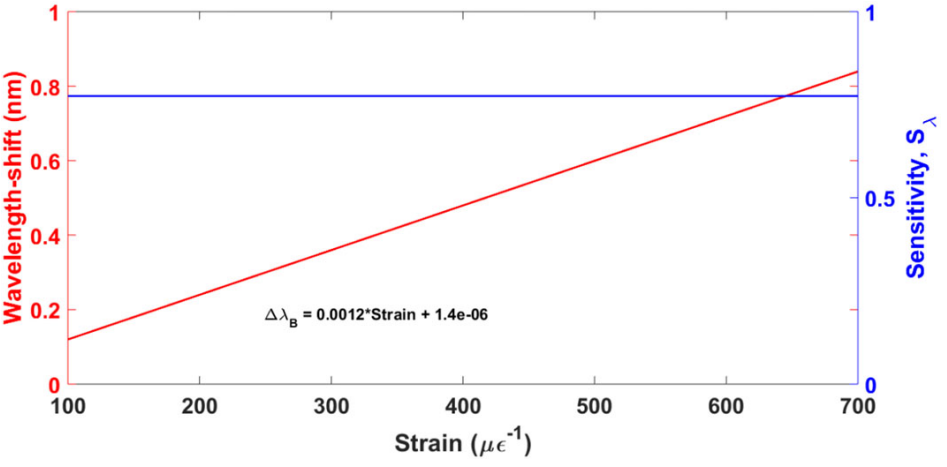

Fig. 7. The Bragg wavelength-shift and sensitivity of optimized π-FBG vs. strain.

the grating length. As previously discussed, to filter out the resonance peak of π-FBG, a suitable apodized FBG filter is required. Recently, we have proposed a new apodization profile $f(z) = J_0(\cos(3z/L))^8(\cos(2z/L-1))^4$, where J_0 is the ordinary Bessel function of the 1st kind of order 0, for the filter and quasi-distributed sensing network [31]. The same apodized grating is applied here for filtering the resonance peak of π-FBG for the illustration. However, other apodized FBG such as Gaussian, raised cosine, Tanh4z, *etc*. may also be used as the filter. The grating parameters are taken as $L = 10$ mm, and $\Delta n = 7 \times 10^{-4}$. The flat-topped bandwidth of the filter is 0.51 nm, which can filter the resonance peak for the ± 200 με US strain amplitudes. The transmitted spectrum of optimized π-FBG, reflectivity spectrum of apodized FBG, and filter output spectrum are shown in Fig. 1. The π-FBG sensor used in [22] is characterized by 1 pm FWHM and peak reflectivity bigger than 99%.

4. Conclusion

The presented numerical investigations show that a π-FBG US sensor exhibits better sensitivity at high frequency as compared to the conventional FBG US sensors. It is because a slow-light effect is observed at the sharp transmission resonance peak, which increases the effective optical path length of light, and, therefore, increased sensitivity is achieved. However, the sensitivity of the system is limited by the interrogating techniques. In this paper, we theoretically analyzed and optimized the US acoustic sensor based on π-FBG and a path imbalance F-MZI interrogation scheme. The optimized proposed sensing system shows the theoretical highest strain sensitivity of $1.2 \times 10^8/\varepsilon$ and a theoretical dynamic strain resolution of 4.1 fε/$\sqrt{\text{Hz}}$. The achieved strain resolution provides a theoretical wavelength shift resolution of 4.9×10^{-9} pm. The strain resolution of the proposed sensing system is much better than 7.3 fε/$\sqrt{\text{Hz}}$ of [25]. A wavelength shift resolution of 3.7×10^{-3} pm is reported in [22] for the acoustic-emission sensor based on the π-FBG and Michelson interferometer. The proposed sensor shows a much better wavelength resolution than the one reported in [22]. The strain sensitivity, resolution, and wavelength-shift sensitivity of the proposed sensing system can further be enhanced by increasing the path mismatch of the F-MZI to the coherent length $\lambda^2/n_{eff}\delta\lambda$, where $\delta\lambda$ is spectral bandwidth of transmission resonance peak of π-FBG. Moreover, the proposed sensing system strongly supports both time and wavelength division multiplexing techniques. Therefore, the proposed sensing system shows extreme importance in single as well as quasi-distributed US acoustic wave sensing networks.

References

[1] Wild, G., Hinckley, S. (2008). Acousto-ultrasonic optical fiber sensors: Overview and state-of-the-art. *IEEE Sensors Journal*, 8(7), 1184–1193.

[2] Teixeira, J.G.V., Leite, I.T., Silva, S., Frazao, O. (2014). Advanced Fiber-Optic Acoustic Sensors. *Photonic Sensors*, 4(3), 198–208.

[3] Zhang, C., Bond, L.J. (2017). Performance Evaluation of the Fiber Bragg Grating (FBG) Sensing Device and Comparison with Piezoelectric Sensors for AE Detection. *AIP Conference Proceedings*, 1806(1).

[4] Wild, G., Hinckley, S. (2010). Optical Fibre Bragg Gratings for Acoustic Sensors. Proceedings of 20th International Congress on Acoustics, ICA 2010, 23–27.

[5] Wee, J. Hackney, D., Bradford, P., Peters, K. (2017). Bi-directional ultrasonic wave coupling to FBGs in continuously bonded optical fiber sensing. *Applied Optics*, 56(25), 7262–7268.

Metrol. Meas. Syst., Vol. 27 (2020), No. 2, pp. 289–300
DOI: 10.24425/mms.2020.132775

[6] Zhao, Y., Zhu, Y., Yuan, M., Wang, J., Zhu, S. (2016). A Laser-Based Fiber Bragg Grating Ultrasonic Sensing System for Structural Health Monitoring. *IEEE Photonics Technology Letters*, 28(22), 2573–2576.

[7] Vidakovic, M., McCague, C., Armakolas, I., Sun, T., Carlton, J.S., Grattan, K.T.V. (2016). Fibre Bragg Grating-Based Cascaded Acoustic Sensors for Potential Marine Structural Condition Monitoring. *Journal of Lightwave Technology*, 34(19), 4473–4478.

[8] Davis, C., Rosalie, C., Norman, P., Rajic, N., Habel, J., Bernier, M. (2018). Remote Sensing of Lamb Waves Using Optical Fibres—An Investigation of Modal Composition. *Journal of Lightwave Technology*, 36(14), 2820–2826.

[9] Xia, M., Jiang, M., Sui, Q., Jia, L. (2015). Theoretical and experimental analysis of interaction from acoustic emission on fiber Bragg grating. *Optik*, 126(11–12), 1150–1155.

[10] Wescley, A.L., Mateus, B.R.C., Taiane, A.M.G.F., Claudia, B.M., Ricardo, M.R. (2018). Low-frequency detection of acoustic signals using fiber as an ultrasonic guide with a distant in-fiber Bragg grating. *Microwave and Optical Technology Letters*, 60(4), 813–817.

[11] Liu, G., Han, M. (2019). Multiplexing fiber-optic ultrasound sensors using laser intensity modulation. *Optics Letters*, 44(4), 751–754.

[12] Minardo, A., Cultrasoundano, A., Bernini, R., Zeni, L., Giordano, M. (2005). Response of fiber Bragg gratings to longitudinal ultrasonic waves. *IEEE Transactions on Ultrasonics, Ferroelectrics, and Frequency Control*, 52(2), 304–312.

[13] Yu, Z., Jiang, Q., Zhang, H., Wang, J. (2016). Theoretical and Experimental Investigation of Fiber Bragg Gratings with Different Lengths for Ultrasonic Detection. *Photonic Sensors*, 6(2), 187–192.

[14] Takeda, N., Okabe, Y., Kuwahara, J., Kojima, S. (2005). Lamb wave sensing using fiber Bragg grating sensors for delamination detection in composite laminates. *Proc. SPIE*, 5758, 135–144.

[15] Liang, S., Tjin, S.C., Lin, B., Sheng, X., Lou, S., Zhang, Y., Wang, X. (2019). Novel Fiber Bragg Grating Sensing Method Based on the Sidelobe Modulation for Ultrasound Detection. *Journal of Lightwave Technology*, 37(11), 2686–2693.

[16] Liu, T., Han, M. (2012). Analysis of π-phase-shifted fiber Bragg gratings for ultrasonic detection. *IEEE Sensors Journal*, 12(7), 2368–2373.

[17] Rosenthal, A., Razansky, D., Ntziachristos, V. (2011). High-sensitivity compact ultrasonic detector based on a pi-phase-shifted fiber Bragg grating. *Optics Letters*, 36(10), 1833–1835.

[18] Dwivedi, K.M., Osuch, T., Trivedi, G. (2019). High Sensitive and Large Dynamic Range Quasi-Distributed Sensing System Based on Slow-Light π-phase-shifted Fiber Bragg Grating. *Opto-Electronics Review*, 27(3), 233–240.

[19] Dwivedi, K. M., Trivedi, G., Osuch, T., Juryca, K., Pidanič, J. (2019). Theoretical Analysis of Slow-light in π-phase-shifted fiber Bragg grating for sensing applications. *Proc. of Conference on Microwave Techniques (COMITE)*, 1–6.

[20] Guo, J., Yang, C. (2015). Highly stabilized phase-shifted fiber Bragg grating sensing system for ultrasonic detection. *IEEE Photonics Technology Letters*, 27(8), 848–851.

[21] Wu, Q., Okabe, Y. (2012). High-sensitivity ultrasonic phase-shifted fiber Bragg grating balanced sensing system. *Optics express*, 20(27), 28353–28362.

[22] Hu, L., Han, M. (2017). Reduction of Laser Frequency Noise and Intensity Noise in Phase-Shifted Fiber Bragg Grating Acoustic-Emission Sensor System. *IEEE Sensors Journal*, 17(15), 4820–4825.

[23] Wu, Q., Okabe, Y. (2012). Ultrasonic sensor employing two cascaded phase-shifted fiber Bragg gratings suitable for multiplexing. *Optics Letters*, 37(16), 3336–3338.

[24] Weis, R.S., Kersey, A.D., Berkoff, T.A. (1994). A Four-Element Fiber Grating Sensor Array with Phase-Sensitive Detection. *IEEE Photonics Technology Letters*, 6(12), 1469–1472.

[25] Koo, K.P., Kersey, A.D. (1995). Bragg Grating-Based Laser Sensors Systems with Interferometric Interrogation and Wavelength Division Multiplexing. *Journal of Lightwave Technology*, 13(7), 1243–1249.

[26] Srivastava, D., Tiwari, U., Das, B. (2018). Interferometric interrogation of π-phase shifted fiber Bragg grating sensors. *Optics Communications*, 410, 88–93.

[27] Yoshino, T., Sano, Y., Ota, D., Fujita, K., Ikui, T. (2016). Fiber-Bragg-Grating Based Single Axial Mode Fabry–Perot Interferometer and Its Strain and Acceleration Sensing Applications. *Journal of Lightwave Technology*, 34(9), 2240–2250.

[28] Chandra, V., Tiwari, U., Das, B. (2016). Elimination of Light Intensity Noise Using Dual-Channel Scheme for Fiber MZI-Based FBG Sensor Interrogation. *IEEE Sensors Journal*, 16(8), 2431–2436.

[29] Erdogan, T. (1997). Fiber Grating Spectra. *Journal of Lightwave Technology*, 15(8), 1277–1294.

[30] Kersey, A.D., Davis M.A., Patrick H.J., LeBlanc M., Koo K.P., Askins C.G., Putnam M.A., and Friebele E.J. (1997). Fiber Grating Sensors. *Journal of Lightwave Technology*, 15(8), 1442–1463.

[31] Dwivedi, K.M., Trivedi, G., Khijwania, S. (2018). Theoretical Analysis of Fiber Bragg Grating Employing Novel Apodization Profile. *Proc. of Photonics*, Photonics 2018, 1–2.